ACS APPLIED ELECTRONIC MATERIALS

pubs.acs.org/acsaelm Article

Highly Anisotropic Thermoelectric Properties of Two-Dimensional As_2Te_3

Zhibin Gao,* Tao Zhu, Kangtai Sun, and Jian-Sheng Wang

Cite This: *ACS Appl. Electron. Mater.* 2021, 3, 1610−1620 Read Online

ACCESS | Metrics & More | Article Recommendations

ABSTRACT: Bulk chalcogenide compounds with chemical formula A_2X_3 (A = As, Sb, Bi, and X = S, Se, Te) are usually semiconductors, topological insulators, and thermoelectric materials. The layers are stacked together *via* weak van der Waals interactions and can be exfoliated into thin two-dimensional (2D) layers. Recently, 2D few-layered As_2S_3 with superior chemical stability was successfully exfoliated in experiments. With a lattice structure to 2D As_2S_3, monolayer As_2Te_3 has a heavier atomic mass and a lower lattice thermal conductivity, which is beneficial to the thermoelectric performance. Here, we study the thermoelectric properties of monolayer As_2Te_3 using *ab initio* calculations combined with semiclassical Boltzmann transport theory. The optimal figure of merit of 2.36 is achieved for hole doping at 600 K, suggesting that monolayer As_2Te_3 is a potential competitor among the efficient and anisotropic thermoelectric materials.

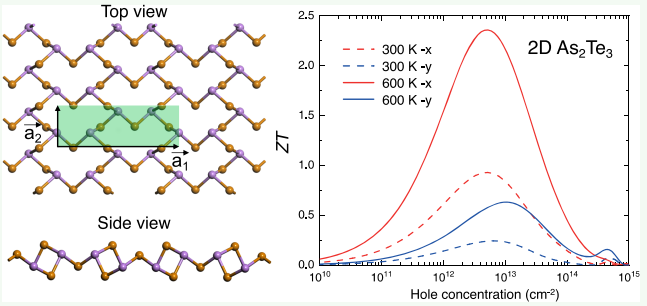

KEYWORDS: *ab initio calculations, 2D As_2Te_3, anisotropic property, figure of merit ZT, thermoelectric property*

INTRODUCTION

Thermoelectric materials can directly and reversibly convert waste heat into electricity. Although it is not as efficient as steam engines and as cheap as pumped thermal salt,[1] thermoelectric materials still have nonreplaceable advantages to generate electrical energy with many promising applications, such as working without noise, isotope thermoelectric generation in aerospace,[2] miniaturization temperature control devices,[3] and even wearable and implantable electronics on the human body.[4] Thermoelectric efficiency can be evaluated by figure of merit $ZT = S^2\sigma T/\kappa$. An optimal thermoelectric material should have a large S, a large σ, and a small κ, simultaneously. However, these parameters are strongly associated with each other. How to relatively decouple the contradictory relation between S and σ is still under exploration, such as through band engineering,[5] machine learning (high-throughput),[6] nanostructuring[7] and so forth. At present, researchers pay much attention to the thermoelectric materials operating across a wide temperature range.[8,9]

Chalcogenide compounds with chemical formula A_2X_3 (A = As, Sb, Bi, and X = S, Se, Te) have been studied in thermoelectric performance for a long time.[10] In the experiment, the highest ZT is 0.65 at 423 K in the Sn-doped As_2Te_3 system.[11] Recently, two-dimensional (2D) materials have stimulated much attention due to their remarkable mechanical, electronic, and phonon properties. Interestingly, as one member of chalcogenide compounds, 2D few-layered As_2S_3 has been successfully peeled off from its bulk counterpart in the experiment in 2019.[12] Besides, some previous works have explored the mechanical, electronic, and optical properties of 2D chalcogenide compounds A_2X_3.[12−15] Considering lattice thermal conductivity is inversely proportional to the effective mass, As_2Te_3 probably has the lowest thermal conductivity in the As_2X_3 compounds, which is favorable to enhance ZT. Furthermore, since 2D As_2Te_3 has a lattice configuration similar to that of As_2S_3, As_2Te_3 has great potential to be exfoliated from the 3D analog.[12] Here, we systematically study the thermoelectric performance of monolayer As_2Te_3, including its band structure, Seebeck coefficient, electrical conductivity, and thermal conductivity, as well as the ZT. We find that As_2Te_3 shows strong anisotropy in electronic, mechanical, and phonon properties. The room-temperature lattice thermal conductivities along the x- and y-axes are 2.76 and 1.68 W/(m K), respectively. A maximum value of ZT being 2.36 for p-type As_2Te_3 at 600 K is obtained in our calculation, suggesting a promising anisotropic thermoelectric performance. The high ZT is derived from "phonon-glass and electron-crystal" that includes the small phonon

Received: December 16, 2020
Accepted: March 23, 2021
Published: April 5, 2021

https://doi.org/10.1021/acsaelm.0c01100
ACS Appl. Electron. Mater. 2021, 3, 1610−1620

velocity, large Grüneisen parameter, small phonon relaxation time, and "pudding-mold" band structure.

THEORETICAL APPROACH

We used PAW pseudopotentials[16,17] and the PBE[18] functional in VASP[19−21] with 550 eV cutoff. The 2D structure has been calculated by a 31 × 31 × 1 Monkhorst−Pack grid.[22] The ionic forces and total energy reach 10^{-4} eV/Å and 10^{-8} eV. The transport properties are obtained by BoltzTraP.[23] To determine the phonon relaxation time, we use 101 × 101 × 1 q-grid. The second-order and third-order interatomic force constants are calculated by Phonopy[24] and ShengBTE.[25] The converged κ_L was obtained after careful testing of the q-grid and cutoff distance. The electronic relaxation time is calculated by the deformation potential (DP) theory.[26]

RESULTS AND DISCUSSION

Crystal Structure and Electronic Structure of As_2Te_3. The optimized monolayer As_2Te_3 is shown in Figure 1a,b. The

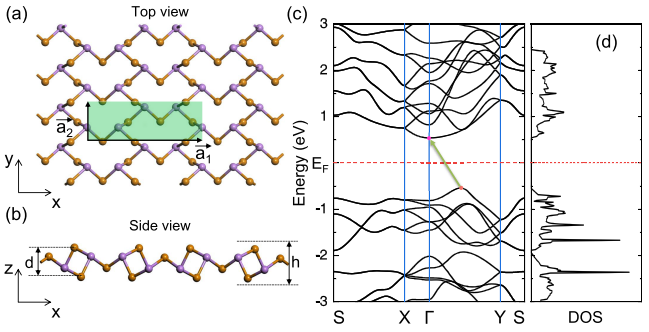

Figure 1. (a, b) Atomic configurations of the monolayer As_2Te_3 in a 2 × 4 supercell. (c) Electronic band structure and (d) electronic density of states (DOS) of As_2Te_3. The Fermi levels are set to zero. Distances d and h shown in panel b represent the intrinsic buckling distance and effective thickness.[27,28] The indirect band gap is indicated by the green arrow in panel c. High-symmetry k points are $S(1/2\ 1/2\ 0)$, $X(1/2\ 0\ 0)$, $\Gamma(0\ 0\ 0)$, and $Y(0\ 1/2\ 0)$, respectively.

equilibrium lattice constants are $|\vec{a_1}|$= 13.097 Å and $|\vec{a_2}|$= 4.510 Å, which are consistent with the previous calculation results of $|\vec{a_1}|$= 13.114 Å and $|\vec{a_2}|$= 4.458 Å.[13] The generic 2D As_2X_3 (X = S, Se, and Te) system possesses the same $Pmn2_1$ symmetry group (space group no. 31) belonging to the orthorhombic system. Up to now, there have been three forms of bulk As_2Te_3: stable α-As_2Te_3 (monoclinic $C2/m$, a = 14.344 Å, b = 4.016 Å, and c = 9.889 Å),[10] metastable β-As_2Te_3 (rhombohedral $R\bar{3}m$, a = 4.0473 Å, and c = 29.5018 Å),[29] and metastable glassy-As_2Te_3.[30] Therefore, our monolayer As_2Te_3 has the potential to be peeled off from the stable bulk α-As_2Te_3 that can be regarded as a composition of monolayer As_2Te_3 assembled by the van der Waals (vdW) interactions.

The intrinsic buckling distance (d) of monolayer As_2Te_3 is 3.254 Å. In low-dimensional materials, since the volume (V) is not a well-defined quantity, one should adopt an effective thickness to compare the related properties with 3D materials, such as mobility and thermal conductivity. Up to now, there have been three different definitions of thickness in 2D materials, including interlayer distance, buckling height between the topmost and bottommost atoms, and the summation of buckling distance and the vdW radii of the outermost surface atoms.[27,28,31] The second choice t_2 has a disadvantage; for instance, the graphene thickness would be zero due to a single carbon layer. We have optimized the bulk As_2Te_3 on the basis of the DFT-D2 method for vdW calculation.[32] The optimized lattice constants are a = 14.399 Å, b = 4.050 Å, and c = 9.846 Å, which are consistent with the previous experimental work with a = 14.344 Å, b = 4.016 Å, and c = 9.889 Å, respectively.[10] Thickness t_1 in our calculation is 7.479 Å, and t_3 of the last definition is 7.374 Å. In most situations, thickness t_3 usually yields a result close to the interlayer distance (t_1) and we adopt t_3 in the following.

For 2D materials, mechanical stability is a critical prerequisite for the applications.[28] There is a 3 × 3 elastic tensor in each 2D materials, which is different from a 6 × 6 elastic tensor in bulk materials. For monolayer As_2Te_3, the calculated C_{11}, C_{12}, C_{22}, and C_{66} are 40.64, 10.50, 13.32, and 15.30 GPa, respectively. If a 2D material is mechanically stable, the corresponding elastic constants have to satisfy $C_{11}C_{22} - C_{12}^2 > 0$ and $C_{66} > 0$. Besides, Young's modulus (E) and Poisson's ratio (ν) of 2D solid materials under the linear response region can be expressed as[27]

$$E_x = \frac{C_{11}C_{22} - C_{12}C_{21}}{C_{22}},\quad E_y = \frac{C_{11}C_{22} - C_{12}C_{21}}{C_{11}},$$
$$\nu_{xy} = \frac{C_{21}}{C_{22}},\quad \nu_{yx} = \frac{C_{12}}{C_{11}} \qquad (1)$$

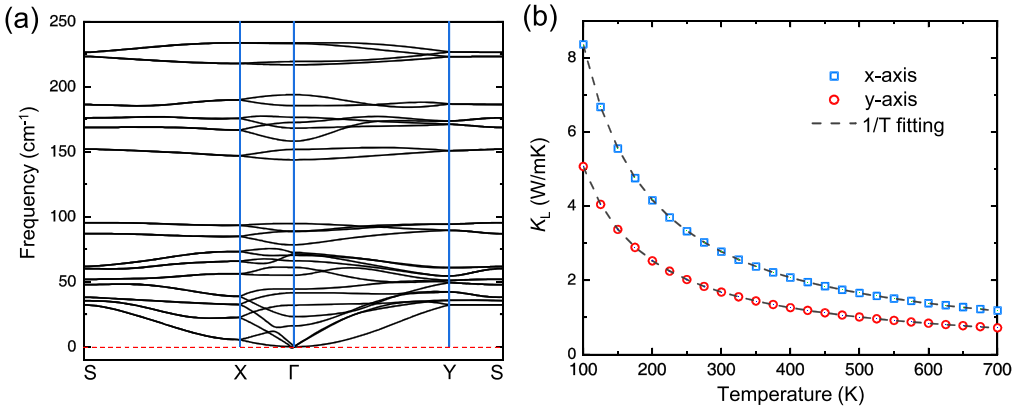

Figure 2. (a) Phonon dispersion of monolayer As_2Te_3. There are three acoustic branches and twenty-seven optical branches. (b) Intrinsic lattice thermal conductivity (κ_L) as a function of the temperature of As_2Te_3. Dashed lines are $1/T$ fittings, which indicate a dominant role of the Umklapp process of phonon−phonon scattering that leads to the thermal resistivity.

https://doi.org/10.1021/acsaelm.0c01100
ACS Appl. Electron. Mater. 2021, 3, 1610−1620

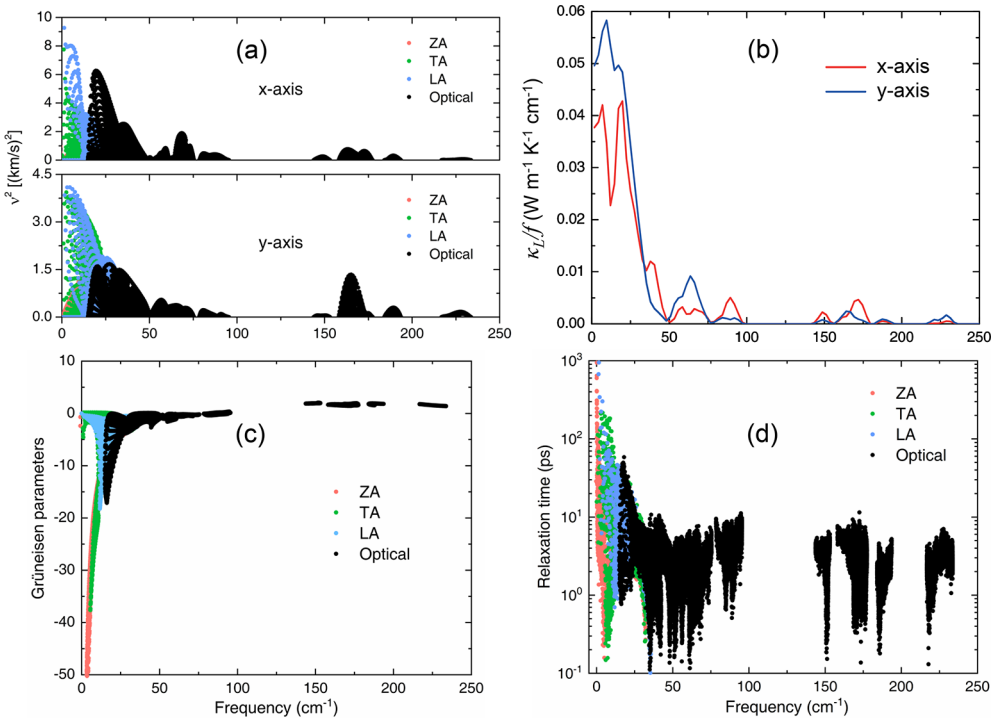

Figure 3. (a) Phonon velocity squared of As_2Te_3 along the *x*-axis and *y*-axis with mode resolution at 300 K. ZA (red), TA (green), and LA (blue) indicate the out-of-plane, in-plane transverse, and in-plane longitudinal phonon modes, respectively. (b) Frequency-resolved κ_L at room temperature along both axes. (c) Grüneisen parameter (γ) as a function of the phonon frequency at 300 K. (d) Three-phonon relaxation time at 300 K.

The calculated Young's moduli E_x and E_y are 32.365 and 10.611 GPa, indicating a higher mechanical hardness in the *x*-axis compared with the *y*-axis. Similarly, the Poisson's ratio ν along x (0.788) and y (0.258) axes also exhibit large mechanical anisotropy.

The electronic band structure and density of state (DOS) distribution for monolayer As_2Te_3 are shown in Figure 1c,d. The conduction band minimum (CBM) locates at the Γ point, while the valence band maximum (VBM) stands between the Γ point and the *Y* point, indicating an indirect band gap property. The electronic transport behavior of monolayer As_2Te_3 is similar to those of As_2S_3 and As_2Se_3 materials.[13] The calculated band gap of monolayer As_2Te_3 is 1.08 eV. More importantly, the valence bands around the Fermi level are relatively flatter than the conduction bands, which lead to a great DOS below the Fermi level shown in Figure 1d. These flat bands will result in a large effective mass. Besides, the Seebeck coefficient is proportional to the effective mass. Therefore, the narrower the electronic band, the larger the effective mass that leads to larger Seebeck coefficients and thermoelectric performance.[33] We will discuss the details in the following.

Thermal Transport Properties of As_2Te_3. Since the ramified relationship between the Seebeck coefficient and the electric conductivity, lattice thermal conductivity (κ_L) becomes a relatively independent parameter in the thermoelectric performance. To explore the thermal transport property of a material, one should divide this problem into two parts. One is harmonic properties and the other is the anharmonic properties. Ultralow κ_L ideally needs weak harmonic and strong anharmonic phonons.[28,34] The computed phonon dispersion of monolayer As_2Te_3 is shown in Figure 2a. It is free from imaginary frequency, indicating the dynamical stability of the monolayer As_2Te_3. There are many flat optical phonon bands above 80 cm^{-1}, indicating small phonon group velocities. There are three acoustic phonons and 27 optical phonons since it has 10 atoms in the primitive cell. Furthermore, there is no acoustic−optical (a−o) gap. The renowned boron arsenide has an ultrahigh κ_L over 2000 W/(m K) at 300 K due to the large a−o gap.[35] Therefore, the material with a small, even a negative, a−o gap is beneficial to minimizing the κ_L owing to the enhancement of scattering between acoustic phonons and optical phonons.[28,36] The optical phonon modes of monolayer As_2Te_3 enter the region belonging to the three acoustic phonon branches, which is an important factor leading to the ultralow κ_L.

In pristine semiconductors and insulators, phonons are the main carrier for heat transport. On the basis of the phonon Boltzmann transport equation (BTE), the lattice thermal conductivity can be calculated by summing the contributions of all phonon modes λ (s, $\mathbf{q}$)[28,34]

$$\kappa_{\alpha\beta} = \frac{1}{V}\sum_{\lambda} C_{\lambda} v_{\lambda\alpha} v_{\lambda\beta} \tau_{\lambda} \tag{2}$$

where C_λ, τ_λ, and $v_{\lambda\,\alpha}$ are the specific heat, phonon relaxation time, and phonon group velocity in the Cartesian direction α of each single-phonon mode, respectively. V is the volume. Figure 2b shows the temperature-dependent κ_L of As_2Te_3 along the *x*- and *y*-axes. Since the phonon anharmonicity becomes stronger, κ_L decreases when the temperature increases. The κ_L of As_2Te_3 material is found to be very low and anisotropic. For instance, the calculated room-temperature κ_L As_2Te_3 along the *x*- and *y*-axes are 2.76 and 1.68 W/(m K), respectively. These values are comparable and even lower than the renowned thermoelectric materials, such as rocksalt PbSe and PbTe whose κ_L were reported in the experiments as low as

https://doi.org/10.1021/acsaelm.0c01100
ACS Appl. Electron. Mater. 2021, 3, 1610−1620

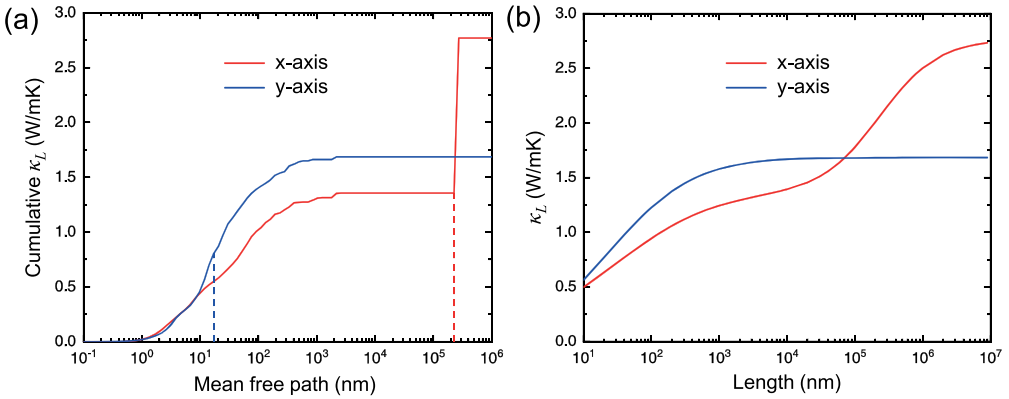

Figure 4. (a) Cumulative lattice thermal conductivity (κ_L) as a function of the phonon mean free path of As_2Te_3 along the *x*-axis and *y*-axis at 300 K. The dashed lines represent cumulative 50% contribution to the total κ_L. (b) κ_L as a function of sample size (L) based on eq 6 at 300 K.

1.7−2.2 W/(m K) at 300 K.[37−39] Moreover, it also the same level of κ_L with the SnSe (0.8, 2.0, and 1.7 W/(m K) along *a*-, *b*-, and *c*-axes, respectively).[40] Note that here κ_L is only considered with phonon−phonon scattering without defects and boundary effects, which would further lead to a small reduction in κ_L for monolayer As_2Te_3. With regard for the anisotropic property, κ_L in the *x*-axis is around 1.6 times larger than that of the *y*-axis, leading to a large anisotropy in the thermal transport of monolayer As_2Te_3. Moreover, we found that κ_L of As_2Te_3 can be well-described by a T^{-1} function (dashed lines in Figure 2b), indicating a dominant Umklapp process of phonon scattering that causes thermal resistivity.

To further unveil the ultralow and anisotropic κ_L of monolayer As_2Te_3, we study the thermal transport behavior physically from both the harmonic and anharmonic properties. Group velocity is one crucial parameter in κ_L from eq 2, which is defined as $\vec{v} = d\omega/d\vec{q}$. The calculated $\vec{v}$ is shown in Figure 3a. In the low-frequency range (<25 cm^{-1}), transverse-acoustic (TA) phonons and longitudinal-acoustic (LA) phonons have large group velocities compared with the flexible-acoustic (ZA) phonons and other optical phonons in both *x*- and *y*-directions. When frequencies increase, TA and LA enter the optical region; thus, the a−o scattering is enhanced significantly. Therefore, the group velocities of TA and LA phonons are suppressed naturally. Besides, group velocities along with the *x*-direction are much larger than those of the *y*-direction, indicating a large anisotropic property of the group velocity.

To explore the specific frequency range in determining κ_L, we show the frequency-resolved κ_L for monolayer As_2Te_3 in Figure 3b. Low-frequency phonons (<50 cm^{-1}) almost dominate the heat transport of κ_L in both the *x*- and *y*-directions. However, acoustic phonons lower than 25 cm^{-1} contribute greater along the *y*-direction (blue line) compared with the *x*-direction (red line). This is consistent with the phonon dispersion shown in Figure 2a. The acoustic phonon branches are softer along Γ−*Y* than Γ−*X* axis. Therefore, acoustic phonons are less disturbed in the Γ−*Y* than that of the Γ−*X* direction, resulting in a large anisotropic κ_L for monolayer As_2Te_3.

The other pivotal parameters in determining κ_L from eq 2 are the phonon relaxation time and anharmonicity, which are highly dependent on the scattering mechanism and intensity in each phonon−phonon scattering channel.[35,41,42] The mode-dependent Grüneisen parameter (γ) is defined as

$$\gamma = -\frac{d \ln \omega}{d \ln V} \tag{3}$$

in which the phonon frequency (ω) is a function of phonon modes (λ) and V is the volume of the crystal. A large γ indicates a large intensity in phonon−phonon scattering modes in materials. The calculated γ of As_2Te_3 is shown in Figure 3c. It is found that acoustic phonon and low-frequency optical phonon branches (<50 cm^{-1}) for As_2Te_3 have large negative γ, while high-frequency optical phonon modes (>50 cm^{-1}) have small positive γ. Like 2D graphene and tellurene, a negative γ usually indicates a negative thermal expansion, which is a favorable property to alleviate the structural thermal stress that will affect the performance of electronic devices in high temperatures.[43,44]

Besides the λ, the total number of phonon−phonon scattering modes is also very important to determine τ_λ from eq 2. Every three-phonon scattering process must satisfy the energy and quasi-momentum conservations expressed as[45,46]

$$\Gamma^{+}_{\lambda\lambda'\lambda''} = \frac{\hbar\pi}{4}\frac{f_0' - f_0''}{\omega_\lambda\omega_{\lambda'}\omega_{\lambda''}}|V^{+}_{\lambda\lambda'\lambda''}|^2\,\delta(\omega_\lambda + \omega_{\lambda'} - \omega_{\lambda''}) \tag{4}$$

$$\Gamma^{-}_{\lambda\lambda'\lambda''} = \frac{\hbar\pi}{4}\frac{f_0' + f_0'' + 1}{\omega_\lambda\omega_{\lambda'}\omega_{\lambda''}}|V^{-}_{\lambda\lambda'\lambda''}|^2\,\delta(\omega_\lambda - \omega_{\lambda'} - \omega_{\lambda''}) \tag{5}$$

where $\Gamma^{-}_{\lambda\lambda'\lambda''}$ and $\Gamma^{+}_{\lambda\lambda'\lambda''}$ represent the emission and absorption rates.[25] The calculated three-phonon relaxation time (τ_λ) at room temperature of monolayer As_2Te_3 is shown in Figure 3d, having an averaged value of 10 ps. Acoustic ZA, TA, and LA phonons have larger τ_λ than that of the optical phonons. As we discussed above, due to the overlap between acoustic phonons and optical phonons shown in Figure 2a around 20 cm^{-1}, the relaxation time of the LA mode and lowest optical phonon branch are highly suppressed, leading to a decreasing tend of κ_L in As_2Te_3. The physical reason behind it is that a larger cross-region of acoustic−optical phonons makes it easier to satisfy the energy and quasi-momentum conservation in eq 4 and eq 5.[28,34,35]

Furthermore, we calculate the cumulative κ_L as a function of phonon mean free path at 300 K in monolayer As_2Te_3, shown in Figure 4a. It is found that cumulative 50% contributions to the total κ_L in monolayer As_2Te_3 are 1.35 and 0.80 W/(m K) along with *x*- and *y*-axes, respectively, indicating a strong anisotropic heat transport in As_2Te_3. The corresponding mean free paths are 2.3×10^5 and 17.1 nm in both axes, respectively.

https://doi.org/10.1021/acsaelm.0c01100
ACS Appl. Electron. Mater. 2021, 3, 1610−1620

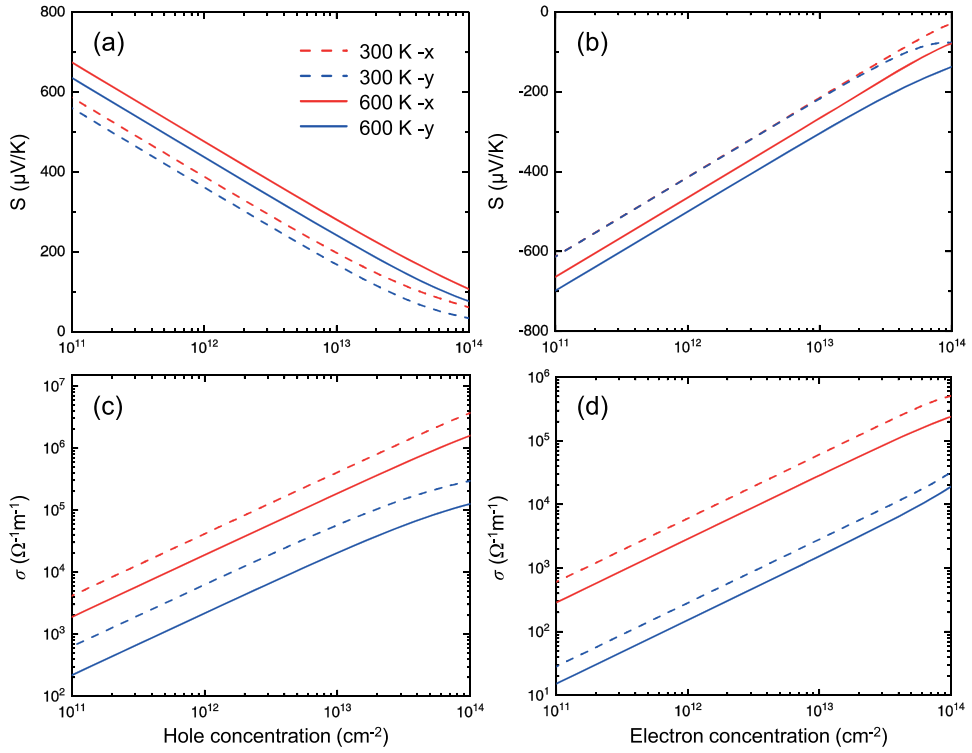

Figure 5. Temperature-dependent electronic transport coefficients. (a, b) Seebeck coefficient (S) and (c, d) electrical conductivity (σ) of the As_2Te_3 as a function of carrier concentration along the *a*- or *b*-axis at 300 and 600 K based on eq 8 and eq 9.

Besides, the size-dependent κ_L is also a factor to affect the thermal transport behavior since the transistors are becoming smaller and smaller. The boundary scattering in the nanomaterials can be evaluated by[47]

$$\frac{1}{\tau_b} = \frac{\upsilon_\lambda}{L} \tag{6}$$

where υ_λ, L, and τ_b are phonon group velocity, material size, and phonon relaxation time of boundary scattering, respectively. According to the Matthiessen's rule, $1/\tau_{total} = 1/\tau_{p-p} + 1/\tau_b$, the boundary scattering can be incorporated into the total phonon relaxation time. The computed total κ_L including boundary scattering of monolayer As_2Te_3 with respect to L is shown in Figure 4b. When L ranges from 10 to 1000 nm, κ_L exhibits a logarithmic function: $\kappa_L \propto \log L$, which is strong evidence of the crucial role of boundary scattering. This phenomenon has been experimentally confirmed in the suspended single-layer graphene previously.[48] For example, when L = 1 nm, κ_L of As_2Te_3 is suppressed to 0.50 and 0.56 W/(m K) along *x*- and *y*-axes, respectively. These are much smaller than that of κ_L of the infinite size. When L increases to 1 μm, κ_L is strengthened to 1.25 and 1.58 W/(m K) along *x*- and *y*-axes, around 45% and 94% along both axes compared with the κ_L of the infinite size. Therefore, our results exhibit different sensitivity along *x*- and *y*-axes and strong anisotropic of heat transport in monolayer As_2Te_3.

As a matter of fact, the length dependence of 2D materials is still under heated debate and different theoretical methods have their own limitations. Molecular dynamics (MD) simulation can consider the full-order phonon−phonon scatterings, but it cannot go beyond the nanoscale larger than 100 μm. The MD simulation should go a longer length to bridge the gap in extracting reliable thermal conductivity. The BTE calculation can well-calculate the size dependence of thermal conductivity even at several millimeters. However, the conventional BTE fails to describe the higher order three-phonon process[49] and collective excitation of phonons.[50,51] Besides, other researchers believe that if the 2D graphene is long enough, the thermal conductivity will probably become diffusive from the ballistic transport, like the nanowire.[52]

Electronic Transport Properties of As_2Te_3. In the framework of Boltzmann transport theory and the relaxation-time approximation, the energy-dependent electronic transport properties, such as Seebeck coefficient (S), electrical conductivity (σ), and electronic thermal conductivity (κ_e), can be obtained by[53]

$$\mathbf{K}_n = \frac{2}{(2\pi)^3}\sum_i \int \mathrm{d}^3\mathbf{k}\, \tau_i(\mathbf{k})\, \mathbf{v}_i(\mathbf{k}) \otimes \mathbf{v}_i(\mathbf{k}) \times [\varepsilon_i(\mathbf{k}) - \mu]^n \left[-\frac{\partial f(\mu, T, \varepsilon_i)}{\partial \varepsilon_i}\right] \tag{7}$$

$$\sigma = e^2\mathbf{K}_0 \tag{8}$$

$$S = \frac{1}{eT}\mathbf{K}_1\mathbf{K}_0^{-1} \tag{9}$$

$$\kappa_e = \frac{1}{T}(\mathbf{K}_2 - \mathbf{K}_1{}^2\mathbf{K}_0^{-1}) \tag{10}$$

where $\mathbf{K}_n$ is a tensor and the coefficient of 2 in eq 7 is the spin degeneracy. The explanation of other parameters can be found elsewhere.[9,54] Besides, the electronic thermal conductivity under open-circuit conditions can also be achieved by the Wiedemann−Franz law,[53]

$$\kappa_e = L\sigma T \tag{11}$$

https://doi.org/10.1021/acsaelm.0c01100
ACS Appl. Electron. Mater. 2021, 3, 1610−1620

Table 1. Calculated Effective Masses (m_x^*/m_0 and m_y^*/m_0), Deformation Potential Constants (E_x and E_y), 2D Elastic Modulus (C_x^{2D} and C_y^{2D}), and Carrier Mobilities (μ_x^{2D} and μ_y^{2D}) Based on Equation 13 for x- and y-axes at 300 K of Monolayer As_2Te_3

carrier type	m_x^*/m_0 (G-X)	m_y^*/m_0 (G-Y)	E_x (eV)	E_y (eV)	C_x^{2D} (J m^{-2})	C_y^{2D} (J m^{-2})	μ_x^{2D} (10^3 m^2 V^{-1} s^{-1})	μ_y^{2D}(10^3 m^2 V^{-1} s^{-1})
electron	0.470	0.201	4.808	7.044	28.052	6.628	0.179	0.046
hole	0.557	1.003	1.554	2.157	28.052	6.628	0.593	0.040

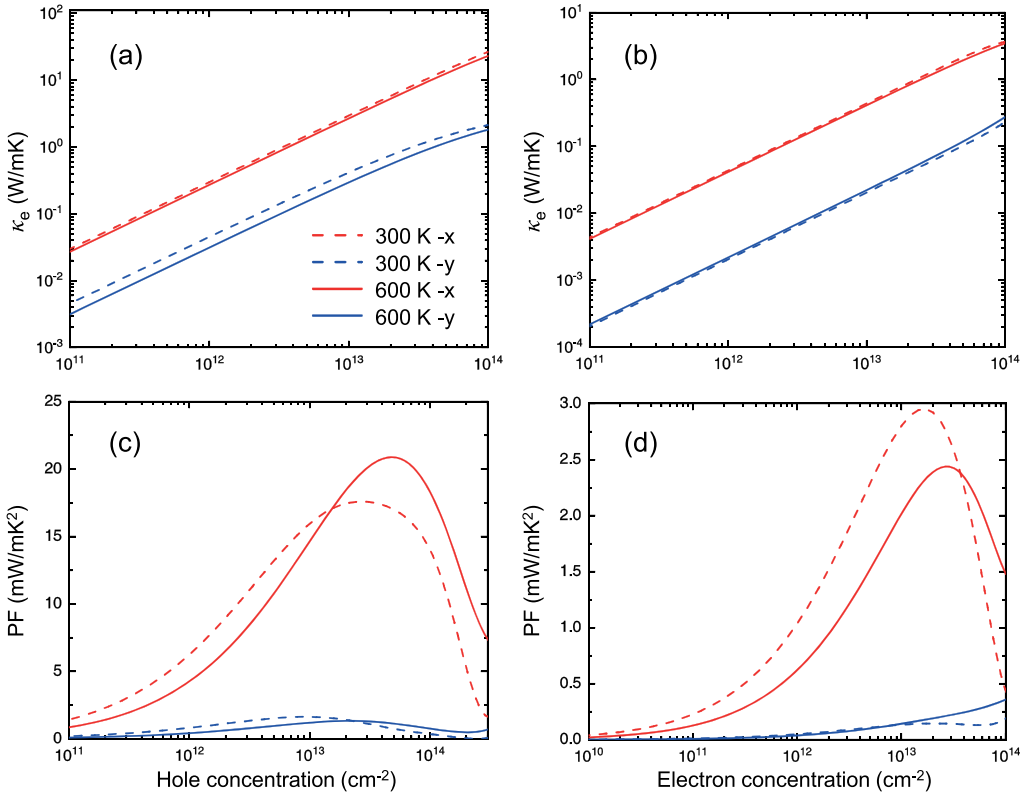

Figure 6. Calculated temperature-dependent (a, b) electronic thermal conductivity (κ_e) and (c, d) power factor ($S^2\sigma$, PF) as a function of temperature and carrier concentration (holes and electrons) along x- and y-axes at 300 and 600 K of As_2Te_3 based on eq 11.

in which L is the Lorenz number with a constant value of 2.4×10^{-8} W Ω K^{-2}. We compare the results of κ_e from eq 10 and eq 11 and find that they are generally consistent with each other. This phenomenon has also been supported by many previous nanomaterials.[9,55,56]

The calculated S and σ for p- and n-type monolayer As_2Te_3 at 300 and 600 K are shown in Figure 5a,b, respectively. S linearly decreases in logarithmic graphs when increasing the carrier concentration for both p- and n-type As_2Te_3. On the basis of the Mohan−Sofo theory, the Seebeck coefficient for 2D semiconductors can be expressed as[33]

$$S_{2D} = \frac{2\pi^3 k_B^2 T}{3eh^2 n} m^*_d \tag{12}$$

in which m_d^* and n are the effective mass of electronic density of states around the Fermi level and carrier concentration, respectively. Therefore, S is inversely proportional to n. Furthermore, S is also proportional to the temperature (T), which can explain why S at 600 K is much larger than that of 300 K. Besides, we can find that S of As_2Te_3 shows strong anisotropic behavior for both p- and n-types. For hole doping, $S_x > S_y$, while $S_y > S_x$ for electron doping. At 10^{12} cm^{-2} hole concentration and 600 K, S is 475 and 436 μV/K for x- and y-axes, respectively. At 10^{12} cm^{-2} electron concentration and 600 K, |S| is 466 and 501 μV/K for x- and y-axes, respectively. These values are around double that of renowned 2D SnSe (200 μV/K) under the same condition.[57]

On the basis of eq 8, the electronic relaxation time (τ) must be given to obtain electric conductivity (σ), since the outcome in BoltzTraP code[53] is σ/τ. In fact, τ is a function of temperature, carrier concentration, and scattering mechanism in given materials. On the one hand, some researchers will approximately adopt a constant relaxation time of 10−12 fs. This strategy has been widely used in recent works.[58−60] On the other hand, τ can be evaluated by the deformation potential (DP) theory which neglects secondarily optical phonons and only considers primarily acoustic phonons in the single parabolic band (SPB) model. In the framework of the DP theory, the acoustic phonon scattering-limited carrier mobility (μ) of 2D materials can be expressed as[9,54]

$$\mu_{2D} = \frac{e\hbar^3 C_{2D}}{k_B T m^* m^*_d E_i^2} \tag{13}$$

where the explanation of parameters can be found elsewhere.[9,54] The electronic relaxation time and carrier mobility have a direct relationship: $\tau = \frac{m^*\mu}{e}$. The calculated effective mass of band (m^*), deformation potential constants (E), and 2D elastic modulus (C^{2D}) are listed in Table 1. The calculated τ are 0.048 and 0.005 ps for electrons in the x- and y-axes,

https://doi.org/10.1021/acsaelm.0c01100
ACS Appl. Electron. Mater. 2021, 3, 1610−1620

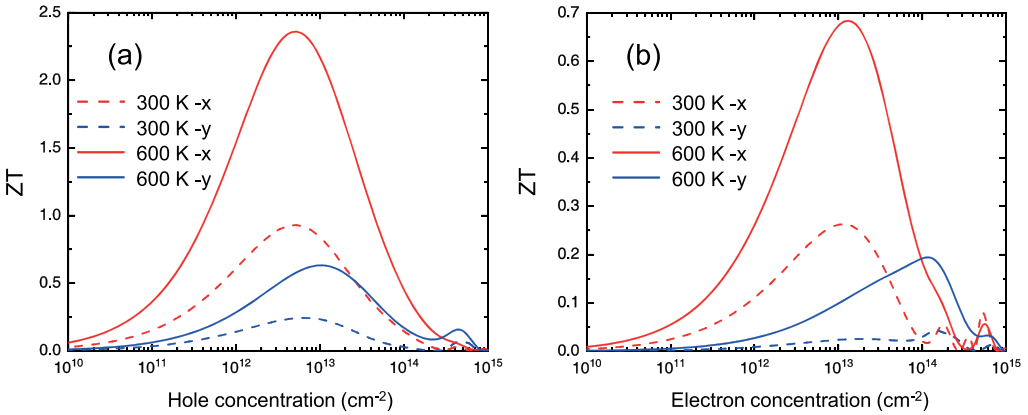

Figure 7. Calculated figure of merit (ZT) of (a) p-type and (b) n-type As_2Te_3 as a function of the carrier concentration along x- and y-axes at 300 and 600 K based on eq 14.

respectively. The corresponding results for holes are 0.188 and 0.023 ps at 300 K. We can find that τ in the y-axis is one order smaller than that of the x-axis, indicating a strong anisotropic electronic property in As_2Te_3. This behavior is reasonable since the crystal structure is softer in the y-axis than x-axis, which is consistent with the lattice formation shown in Figure 1a,b. Although the DP theory has been a great success, the relaxation time, in principle, should also relate to the doping concentration. More details are discussed in Appendix.

On the basis of the result of electronic relaxation time, anisotropic σ are given in Figure 5a,b. In general, σ for both p- and n-type As_2Te_3 increases as the carrier concentration rises. Anisotropic σ is confirmed at 300 and 600 K in all carrier concentrations. σ along with the x-axis is around 1 order of magnitude larger than that of the y-axis owing to the anisotropic relaxation time. Depending on eq 11, κ_e is plotted in Figure 6a,b. Since κ_e and σ are positive and linearly connected, κ_e for both p- and n-type As_2Te_3 are proportional to the carrier concentrations. Besides, κ_e is not sensitive to the temperature according to our calculation. With hole concentration being 10^{13} cm^{-2} at 300 K, κ_e are 3.32 and 0.46 W/(m K) along x- and y-axes, respectively. κ_L are 2.76 and 1.68 W/(m K), respectively, under the same condition. Therefore, both κ_e and κ_L are essential for thermal transport and thermoelectric performance.

The power factor (PF, $S^2\sigma$) in Figure 6c,d exhibits the final balance of contradiction relation between S and σ as a function of carrier concentration. PF first increases at low concentration and then decreases at high concentration. It is clearly found that PF in the x-axis (red) is quite larger than that in the y-axis (blue). Furthermore, p-type As_2Te_3 possesses a significantly higher PF than that of the n-type situation. The highest value of p-type As_2Te_3 is 17.59 (20.87) mW/(m K^2) along the x-axis at 300 (600) K with the hole concentrations of 2.74×10^{13} (4.72×10^{13}) cm^{-2}. On the contrary, for the n-type doping, the maximum PF values are 2.95 (2.43) mW/(m K^2) along the x-axis at 300 (600) K with the electron concentration of 1.73×10^{13} (2.64×10^{13}) cm^{-2}. Such high values of the PF are comparable to other renowned thermoelectric materials, such as layered LaCuOSe (3.0 mW/(m K^2)),[55] tellurene (57.3 mW/(m K^2)),[54] and PbTe (2.5 mW/(m K^2)).[61]

Figure of Merit (ZT). With all of the above results of phonon and electron transport properties, ZT can be determined as

$$ZT = \frac{S^2\sigma}{\kappa_e + \kappa_L} T \tag{14}$$

The results are shown in Figure 7a,b, respectively. Evidently, ZT is highly anisotropic due to the orientation-dependent transport properties of phonons and electrons. Because of the high power factor and low lattice thermal conductivity, monolayer As_2Te_3 demonstrates a ZT value larger than 2 at 600 K for the hole doping. The maximum values of ZT in the x-axis are 2.36 and 0.93 for hole concentration of about 5.25×10^{12} cm^{-2} at 600 and 300 K, respectively. On the other hand, the highest value of ZT in the x-axis is 0.68 for electron concentration of about 1.30×10^{13} cm^{-2} at 600 K. The obtained high ZT of As_2Te_3, especially for p-type doping, is derived from the elevated S and σ, as well as the reduced κ_L along the x-axis. Such a high ZT being 2.36 for p-type As_2Te_3 is comparable to the 0.83 at 700 K in tellurene,[54] 2.78 at 800 K in $GeAs_2$,[56] 2.71 at 900 K in LaCuOSe,[55] and 2.6 at 923 K in SnSe.[62] Therefore, our results show that monolayer As_2Te_3 is a superior thermoelectric material, particularly for p-type doping.

The highest ZT originates from the hole carrier, corresponding to the valence bands. We have observed that the valence bands around the Fermi level are highly degenerate, while conduction bands are nondegenerate shown in Figure 1c, leading to the famous pudding-mold band structure[63] that will increase $S^2\sigma$ significantly and finally upgrade the ZT of monolayer As_2Te_3.

CONCLUSIONS

In summary, we have systematically investigated the thermoelectric properties of monolayer arsenic telluride As_2Te_3 by *ab initio* calculations and Boltzmann transport theory. The lattice formation, electronic band structure, phonon dispersion, Seebeck coefficient, electric conductivity, electronic thermal conductivity, and lattice thermal conductivity of As_2Te_3 show a large anisotropy between the x- and y-axes. p-type and n-type dopings also exhibit anisotropic behavior. The room-temperature κ_L along the x- and y-axes are 2.76 and 1.68 W/(m K), respectively. This is mainly ascribed to the strong scattering between acoustic phonons and optical phonons. Our results exhibit that a large power factor of 17.59 (20.87) mW/(m K^2) along the x-axis can be achieved at 300 (600) K with the hole concentration of 2.74×10^{13} (4.72×10^{13}) cm^{-2}. Owing to the ultralow lattice thermal conductivity and large power factor, a maximum value of ZT being 2.36 can be obtained for p-type

https://doi.org/10.1021/acsaelm.0c01100
ACS Appl. Electron. Mater. 2021, 3, 1610−1620

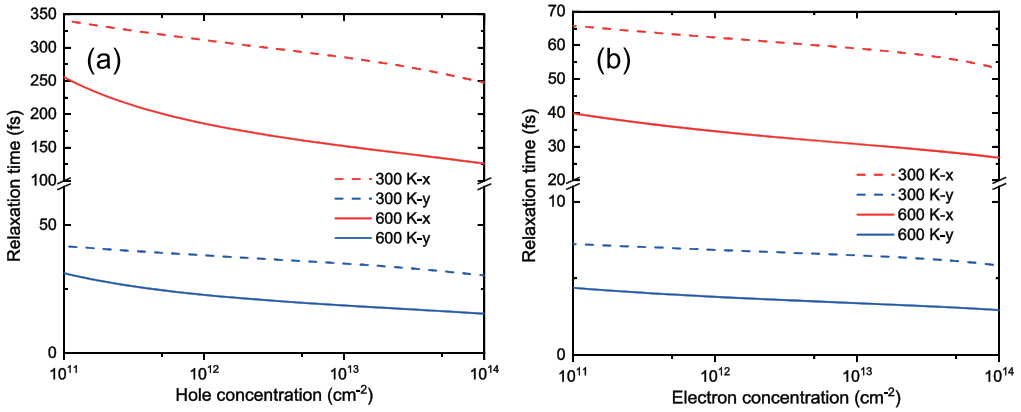

Figure 8. Calculated relaxation time ($\tau_{2D}^{a\text{-}ph}$) as a function of temperature and carrier concentration for (a) holes and (b) electrons in monolayer As_2Te_3 based on eq 15 and eq 21.

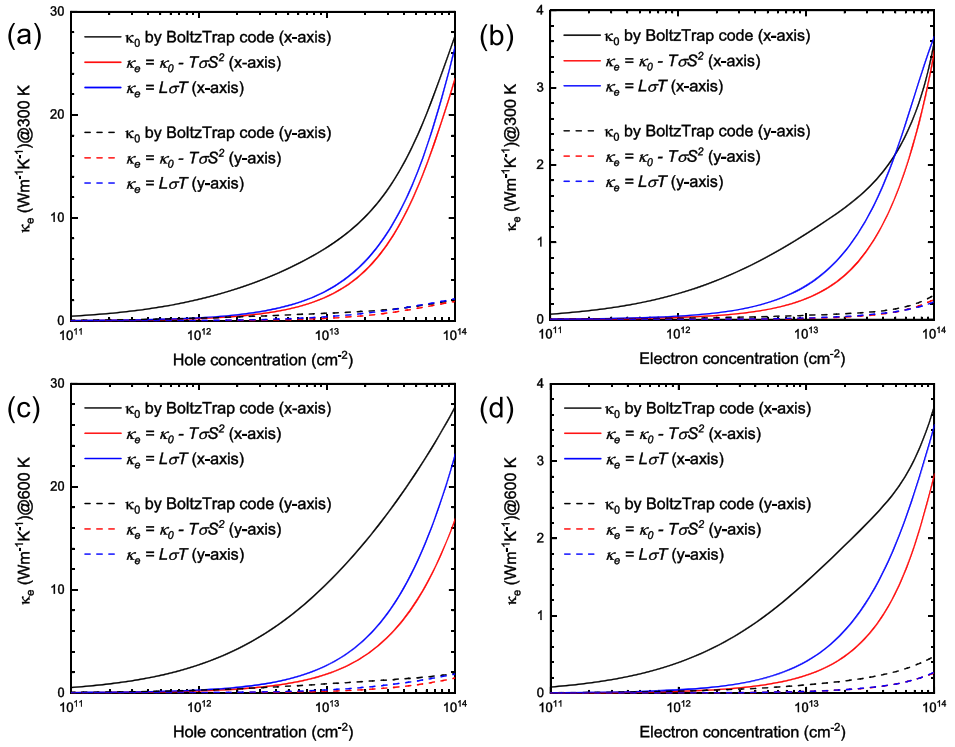

Figure 9. Calculated electronic thermal conductivity (κ_e) for monolayer As_2Te_3 at a function of temperature and carrier concentration: (a) 300 K for holes, (b) 300 K for electrons, (c) 600 K for holes, and (d) 600 K for electrons, respectively. Two methods are the Wiedemann−Franz law from eq 11 and the definition from eq 10 and eq 22.

As_2Te_3 at 600 K in the *x*-axis. Our study indicates that monolayer As_2Te_3 has strong anisotropic behaviors in phonon and electronic transport properties. Our work also suggests that monolayer As_2Te_3 is a promising material for thermoelectric applications, especially operating across a wide temperature range.

APPENDIX: DOPING-DEPENDENT RELAXATION TIME AND THERMAL CONDUCTIVITY

In the framework of DP theory, the doping-dependent relaxation time is defined as

$$\tau = \tau_0 E^r \tag{15}$$

in which *r* can possess several values based on the different scattering mechanisms, including longitudinal-acoustic phonons (−1/2), nonpolar optical phonons (1/2), polar optical phonons (1/2), and ionized impurities (3/2), respectively. *E* is the energy of the electron. Generally, the scattering between longitudinal-acoustic phonons and electrons can well-describe most materials, such as nonpolar crystals,[26] carbon and organic nanomaterials,[64] 2D graphene,[65] monolayer MoS_2 nanoribbons,[66] anisotropic 2D SiS,[67] and anisotropic 2D tellurene.[68]

The parameter τ_0 in eq 15 for 3D materials has different expressions dependent on the type of scattering:[69,70]

$$\tau_0^{a\text{-}ph} = \frac{h^4}{8\pi^3}\frac{\rho {v_L}^2}{k_B T}\frac{1}{(2m^*)^{3/2}D^2} \tag{16}$$

$$\tau_0^{o\text{-}ph(nonpolar)} = \frac{h^2}{2^{1/2}(m^*)^{1/2}e^2 k_B T({\varepsilon_\infty}^{-1} - {\varepsilon_0}^{-1})} \tag{17}$$

https://doi.org/10.1021/acsaelm.0c01100
ACS Appl. Electron. Mater. 2021, 3, 1610−1620

$$\tau_0^{\text{o-ph(polar)}} = \frac{h^2}{2^{1/2}(m^*)^{1/2}e^2k_BT(\varepsilon_\infty^{-1} - \varepsilon_0^{-1})} \times \frac{1}{[1 - \delta_\infty \ln(1 + \delta_\infty^{-1})]} \quad (18)$$

$$\tau_0^{\text{imp}} = \left[\frac{Z^2e^4N_i}{16\pi(2m^*)^{1/2}\varepsilon^2} \ln\left[1 + \left(\frac{2E}{E_m}\right)^2\right]\right]^{-1} \quad (19)$$

where $\tau_0^{\text{a-ph}}$, $\tau_0^{\text{o-ph(nonpolar)}}$, $\tau_0^{\text{o-ph(polar)}}$, and τ_0^{imp} are the carrier scattering constants for the acoustic phonons, nonpolar optical phonons, polar optical phonons, and ionized impurities, respectively.

Note that the above formulas are exclusively applicable to 3D materials. Up to now, researchers have only found and verified the relaxation time obtained from the scattering model between electrons and longitudinal-acoustic phonons in 2D materials. The corresponding $\tau^{\text{a-ph}}$ is

$$\tau_{3D}^{\text{a-ph}} = \frac{h^4}{8\pi^3}\frac{C_{3D}}{k_BT}\frac{1}{(2m^*)^{3/2}D^2}E^{-1/2} \quad (20)$$

$$\tau_{2D}^{\text{a-ph}} = \frac{h^3}{8\pi^3}\frac{C_{2D}}{k_BT}\frac{1}{m^*D^2}E^{-1/2} \quad (21)$$

Here, we have calculated the relaxation time of monolayer As_2Te_3 according to eq 21, shown in Figure 8. We find that the relaxation time $(\tau)_{2D}^{\text{a-ph}}$ slightly decreases when increasing the carrier (holes or electrons) concentration, which is reasonable due to the enhanced population of carrier leading to a stronger electron−phonon scattering.[71]

On the basis of the relaxation time, one can get the electronic thermal conductivity from the BoltzTraP code rather than the Wiedemann−Franz law where the Lorenz number sometimes varies slightly in different systems. Therefore, the electronic thermal conductivity, κ_e, is written as[23]

$$\kappa_e = \kappa_0 - T\sigma S^2 \quad (22)$$

in which κ_0 is the electronic thermal conductivity obtained directly using the BoltzTraP. T, S, and σ are the absolute temperature, Seebeck coefficient, and electric conductivity, respectively. The calculated results from the two methods are shown in Figure 9.

As we can see κ_e obtained from the Wiedemann−Franz law and the BoltztraP code agree very well with each other no matter the type of carrier (electrons or holes). Furthermore, κ_e received from the Wiedemann−Franz law (red lines) is always slightly larger than that of results using the definition (blue lines) for 2D monolayer As_2Te_3.

Note that other scattering from nonpolar optical phonons, polar optical phonons, and ionized impurities cannot be easily transplanted into formulas for 2D materials. The physical reason is the order of effective mass. In 3D materials, there are three linear acoustic phonon modes, whereas in 2D, there are only two linear modes (TA and LA) and one quadratic ZA acoustic phonon mode whose vibration direction is out-of-plane. For 2D materials, in the long-wavelength limit, very close to the Γ point, the LA and TA phonon modes are linear in wave vector **q**, whereas the ZA mode is quadratic, with coefficients given by 2D continuum elasticity theory. But when **q** is slightly far away from Γ point, ZA mode will have a near-linear trend, leading to a complex situation in 2D transport problem. Therefore, estimation the effect of optical phonons and impurities on the mobility is beyond the scope of our capability in this work.

We think due to the unique behavior of the ZA mode of 2D materials, leading to a totally different formula of phonon dispersion and phonon density of states, one single formula to calculate the relaxation time for 2D materials is not suitable. One should divide the total scattering into two parts; one is TA and LA phonons, and the other one is the special ZA phonon. The previous part (TA and LA phonons) could use the conventional 3D formula. However, the latter part (ZA phonon) is still an open question that deserves further study and exploration.

Alternatively, one can also obtain the electronic relaxation time from *ab initio* calculation, such as EPW[72] and Perturbo[73] based on the DFPT and Wannier interpolation methods. Compared with the conventional model, first principles calculation is more accurate but more expansive. Balanced methods with moderate precision and efficiency are further needed. We hope machine-learning method may shed new light on this field in the new future.

AUTHOR INFORMATION

Corresponding Author

Zhibin Gao − *State Key Laboratory for Mechanical Behavior of Materials, Xi'an Jiaotong University, Xi'an 710049, China*; orcid.org/0000-0002-6843-381X; Email: zhibingao@outlook.com

Authors

Tao Zhu − *Department of Physics, National University of Singapore, Singapore 117551, Republic of Singapore*

Kangtai Sun − *Department of Physics, National University of Singapore, Singapore 117551, Republic of Singapore*

Jian-Sheng Wang − *Department of Physics, National University of Singapore, Singapore 117551, Republic of Singapore*

Complete contact information is available at: https://pubs.acs.org/10.1021/acsaelm.0c01100

Notes

The authors declare no competing financial interest.

ACKNOWLEDGMENTS

We thank Jin-Jian Zhou from California Institute of Technology and Jinyang Xi from Shanghai University for their inspiring discussions and valuable suggestions. We acknowledge the financial support from MOE tier 1 funding of Singapore (Grant No. R-144-000-427-114).

REFERENCES

(1) Vining, C. B. An inconvenient truth about thermoelectrics. *Nat. Mater.* **2009**, *8*, 83−85.

(2) Bankston, C.; Cole, T.; Jones, R.; Ewell, R. Experimental and systems studies of the alkali metal thermoelectric converter for aerospace power. *J.Energy* **1983**, *7*, 442−448.

(3) Han, C.-G.; Qian, X.; Li, Q.; Deng, B.; Zhu, Y.; Han, Z.; Zhang, W.; Wang, W.; Feng, S.-P.; Chen, G.; Liu, W. Giant thermopower of ionic gelatin near room temperature. *Science* **2020**, *368*, 1091−1098.

(4) Wang, Y.; Yang, L.; Shi, X.-L.; Shi, X.; Chen, L.; Dargusch, M. S.; Zou, J.; Chen, Z.-G. Flexible thermoelectric materials and generators: challenges and innovations. *Adv. Mater.* **2019**, *31*, 1807916.

(5) Pei, Y.; Wang, H.; Snyder, G. J. Band engineering of thermoelectric materials. *Adv. Mater.* **2012**, *24*, 6125−6135.

(6) Yan, S.; Wang, Y.; Gao, Z.; Long, Y.; Ren, J. Directional Design of Materials Based on Multi-Objective Optimization: A. Case Study of Two-Dimensional Thermoelectric SnSe. *Chin. Phys. Lett.* **2021**, *38* (2), 027301.
(7) Snyder, G.; Toberer, E. Complex Thermoelectric Materials. *Nat. Mater.* **2008**, *7*, 105−114.
(8) Xiao, Y.; Zhao, L.-D. Seeking new, highly effective thermoelectrics. *Science* **2020**, *367*, 1196−1197.
(9) Gao, Z.; Wang, J.-S. Thermoelectric Penta-Silicene with a High Room-Temperature Figure of Merit. *ACS Appl. Mater. Interfaces* **2020**, *12*, 14298−14307.
(10) Cuenca-Gotor, V. P.; Sans, J. A.; Ibáñez, J.; Popescu, C.; Gomis, O.; Vilaplana, R.; Manjón, F. J.; Leonardo, A.; Sagasta, E.; Suárez-Alcubilla, A.; Gurtubay, I. G.; Mollar, M.; Bergara, A. Structural, vibrational, and electronic study of α-As_2Te_3 under compression. *J. Phys. Chem. C* **2016**, *120*, 19340−19352.
(11) Vaney, J.-B.; Carreaud, J.; Delaizir, G.; Pradel, A.; Piarristeguy, A.; Morin, C.; Alleno, E.; Monnier, J.; Gonçalves, A. P.; Candolfi, C.; Dauscher, A.; Lenoir, B. High-Temperature Thermoelectric Properties of Sn-Doped β-As_2Te_3. *Adv. Electron. Mater.* **2015**, *1*, 1400008.
(12) šiškins, M.; Lee, M.; Alijani, F.; van Blankenstein, M. R.; Davidovikj, D.; van der Zant, H. S.; Steeneken, P. G. Highly Anisotropic Mechanical and Optical Properties of 2D Layered As_2S_3 Membranes. *ACS Nano* **2019**, *13*, 10845−10851.
(13) Mortazavi, B.; Shojaei, F.; Azizi, M.; Rabczuk, T.; Zhuang, X. As_2S_3, As_2Se_3 and As_2Te_3 nanosheets: superstretchable semiconductors with anisotropic carrier mobilities and optical properties. *J. Mater. Chem. C* **2020**, *8*, 2400−2410.
(14) Miao, N.; Zhou, J.; Sa, B.; Xu, B.; Sun, Z. Few-layer arsenic trichalcogenides: Emerging two-dimensional semiconductors with tunable indirect-direct band-gaps. *J. Alloys Compd.* **2017**, *699*, 554−560.
(15) Debbichi, L.; Kim, H.; Björkman, T.; Eriksson, O.; Lebègue, S. First-principles investigation of two-dimensional trichalcogenide and sesquichalcogenide monolayers. *Phys. Rev. B: Condens. Matter Mater. Phys.* **2016**, *93*, 245307.
(16) Blöchl, P. E. Projector augmented-wave method. *Phys. Rev. B: Condens. Matter Mater. Phys.* **1994**, *50*, 17953−17979.
(17) Kresse, G.; Joubert, D. From ultrasoft pseudopotentials to the projector augmented-wave method. *Phys. Rev. B: Condens. Matter Mater. Phys.* **1999**, *59*, 1758−1775.
(18) Perdew, J. P.; Burke, K.; Ernzerhof, M. Generalized Gradient Approximation Made Simple. *Phys. Rev. Lett.* **1996**, *77*, 3865−3868.
(19) Kresse, G.; Furthmüller, J. Efficient iterative schemes for ab initio total-energy calculations using a plane-wave basis set. *Phys. Rev. B: Condens. Matter Mater. Phys.* **1996**, *54*, 11169−11186.
(20) Kresse, G.; Furthmüller, J. Efficiency of ab-initio total energy calculations for metals and semiconductors using a plane-wave basis set. *Comput. Mater. Sci.* **1996**, *6*, 15−50.
(21) Kresse, G.; Hafner, J. *Ab initio* molecular-dynamics simulation of the liquid-metal-amorphous-semiconductor transition in germanium. *Phys. Rev. B: Condens. Matter Mater. Phys.* **1994**, *49*, 14251−14269.
(22) Monkhorst, H. J.; Pack, J. D. Special points for Brillouin-zone integrations. *Phys. Rev. B* **1976**, *13*, 5188−5192.
(23) Madsen, G. K.; Singh, D. J. BoltzTraP. A code for calculating band-structure dependent quantities. *Comput. Phys. Commun.* **2006**, *175*, 67−71.
(24) Togo, A.; Oba, F.; Tanaka, I. First-principles calculations of the ferroelastic transition between rutile-type and $CaCl_2$-type SiO_2 at high pressures. *Phys. Rev. B: Condens. Matter Mater. Phys.* **2008**, *78*, 134106.
(25) Li, W.; Carrete, J.; Katcho, N. A.; Mingo, N. ShengBTE: A solver of the Boltzmann transport equation for phonons. *Comput. Phys. Commun.* **2014**, *185*, 1747−1758.
(26) Bardeen, J.; Shockley, W. Deformation Potentials and Mobilities in Non-Polar Crystals. *Phys. Rev.* **1950**, *80*, 72−80.
(27) Gao, Z.; Dong, X.; Li, N.; Ren, J. Novel two-dimensional silicon dioxide with in-plane negative Poisson's ratio. *Nano Lett.* **2017**, *17*, 772−777.
(28) Gao, Z.; Tao, F.; Ren, J. Unusually low thermal conductivity of atomically thin 2D tellurium. *Nanoscale* **2018**, *10*, 12997−13003.
(29) Vaney, J.-B.; Carreaud, J.; Delaizir, G.; Morin, C.; Monnier, J.; Alleno, E.; Piarristeguy, A.; Pradel, A.; Goncalves, A. P.; Lopes, E. B.; Candolfi, C.; Dauscher, A.; Lenoir, B. Thermoelectric Properties of the α-As_2Te_3 Crystalline Phase. *J. Electron. Mater.* **2016**, *45*, 1447−1452.
(30) Cornet, J.; Rossier, D. Properties and structure of As-Te glasses:(I). Glass-forming ability and related properties. *J. Non-Cryst. Solids* **1973**, *12*, 61−84.
(31) Wu, X.; Varshney, V.; Lee, J.; Pang, Y.; Roy, A. K.; Luo, T. How to characterize thermal transport capability of 2D materials fairly?-Sheet thermal conductance and the choice of thickness. *Chem. Phys. Lett.* **2017**, *669*, 233−237.
(32) Grimme, S. Semiempirical GGA-type density functional constructed with a long-range dispersion correction. *J. Comput. Chem.* **2006**, *27*, 1787−1799.
(33) Heremans, J. P.; Jovovic, V.; Toberer, E. S.; Saramat, A.; Kurosaki, K.; Charoenphakdee, A.; Yamanaka, S.; Snyder, G. J. Enhancement of Thermoelectric Efficiency in PbTe by Distortion of the Electronic Density of States. *Science* **2008**, *321*, 554−557.
(34) Gao, Z.; Zhang, Z.; Liu, G.; Wang, J.-S. Ultra-low lattice thermal conductivity of monolayer penta-silicene and penta-germanene. *Phys. Chem. Chem. Phys.* **2019**, *21*, 26033−26040.
(35) Lindsay, L.; Broido, D. A.; Reinecke, T. L. First-Principles Determination of Ultrahigh Thermal Conductivity of Boron Arsenide: A Competitor for Diamond? *Phys. Rev. Lett.* **2013**, *111*, 025901.
(36) Delaire, O.; Ma, J.; Marty, K.; May, A. F.; McGuire, M. A.; Du, M.-H.; Singh, D. J.; Podlesnyak, A.; Ehlers, G.; Lumsden, M.; Sales, B. C. Giant anharmonic phonon scattering in PbTe. *Nat. Mater.* **2011**, *10*, 614−619.
(37) Sootsman, J. R.; Chung, D. Y.; Kanatzidis, M. G. New and old concepts in thermoelectric materials. *Angew. Chem., Int. Ed.* **2009**, *48*, 8616−8639.
(38) Wang, H.; Pei, Y.; LaLonde, A. D.; Snyder, G. J. Heavily doped p-type PbSe with high thermoelectric performance: an alternative for PbTe. *Adv. Mater.* **2011**, *23*, 1366−1370.
(39) El-Sharkawy, A.; Abou El-Azm, A.; Kenawy, M.; Hillal, A.; Abu-Basha, H. Thermophysical properties of polycrystalline PbS, PbSe, and PbTe in the temperature range 300−700 K. *Int. J. Thermophys.* **1983**, *4*, 261−269.
(40) Guo, R.; Wang, X.; Kuang, Y.; Huang, B. First-principles study of anisotropic thermoelectric transport properties of IV-VI semiconductor compounds SnSe and SnS. *Phys. Rev. B: Condens. Matter Mater. Phys.* **2015**, *92*, 115202.
(41) Holland, M. G. Phonon Scattering in Semiconductors From Thermal Conductivity Studies. *Phys. Rev.* **1964**, *134*, A471−A480.
(42) Slack, G. A. Nonmetallic crystals with high thermal conductivity. *J. Phys. Chem. Solids* **1973**, *34*, 321−335.
(43) Yoon, D.; Son, Y.-W.; Cheong, H. Negative thermal expansion coefficient of graphene measured by Raman spectroscopy. *Nano Lett.* **2011**, *11*, 3227−3231.
(44) Liu, G.; Gao, Z.; Ren, J. Anisotropic thermal expansion and thermodynamic properties of monolayer β-Te. *Phys. Rev. B: Condens. Matter Mater. Phys.* **2019**, *99*, 195436.
(45) Lindsay, L.; Broido, D. Three-phonon phase space and lattice thermal conductivity in semiconductors. *J. Phys.: Condens. Matter* **2008**, *20*, 165209.
(46) Lee, S.; Esfarjani, K.; Luo, T.; Zhou, J.; Tian, Z.; Chen, G. Resonant bonding leads to low lattice thermal conductivity. *Nat. Commun.* **2014**, *5*, 3525.
(47) Balandin, A. A.; Ghosh, S.; Bao, W.; Calizo, I.; Teweldebrhan, D.; Miao, F.; Lau, C. N. Superior thermal conductivity of single-layer graphene. *Nano Lett.* **2008**, *8*, 902−907.
(48) Xu, X.; Pereira, L. F. C.; Wang, Y.; Wu, J.; Zhang, K.; Zhao, X.; Bae, S.; Tinh Bui, C.; Xie, R.; Thong, J. T. L.; Hong, B. H.; Loh, K. P.;

https://doi.org/10.1021/acsaelm.0c01100
ACS Appl. Electron. Mater. 2021, 3, 1610−1620

Donadio, D.; Li, B.; Özyilmaz, B. Length-dependent thermal conductivity in suspended single-layer graphene. *Nat. Commun.* **2014**, *5*, 3689.
(49) Tadano, T.; Tsuneyuki, S. Self-consistent phonon calculations of lattice dynamical properties in cubic $SrTiO_3$ with first-principles anharmonic force constants. *Phys. Rev. B: Condens. Matter Mater. Phys.* **2015**, *92*, 054301.
(50) Cepellotti, A.; Marzari, N. Thermal Transport in Crystals as a Kinetic Theory of Relaxons. *Phys. Rev. X* **2016**, *6*, 041013.
(51) Cepellotti, A.; Fugallo, G.; Paulatto, L.; Lazzeri, M.; Mauri, F.; Marzari, N. Phonon hydrodynamics in two-dimensional materials. *Nat. Commun.* **2015**, *6*, 6400.
(52) Vakulov, D.; et al. Ballistic Phonons in Ultrathin Nanowires. *Nano Lett.* **2020**, *20*, 2703−2709.
(53) Madsen, G. K.; Singh, D. J. A Code for Calculating Band-Structure Dependent Quantities. *Comput. Phys. Commun.* **2006**, *175*, 67−71.
(54) Gao, Z.; Liu, G.; Ren, J. High Thermoelectric Performance in Two-Dimensional Tellurium: An Ab Initio Study. *ACS Appl. Mater. Interfaces* **2018**, *10*, 40702−40709.
(55) Wang, N.; Li, M.; Xiao, H.; Zu, X.; Qiao, L. Layered LaCuOSe: APromising Anisotropic Thermoelectric Material. *Phys. Rev. Appl.* **2020**, *13*, 024038.
(56) Wang, F. Q.; Guo, Y.; Wang, Q.; Kawazoe, Y.; Jena, P. Exceptional Thermoelectric Properties of Layered $GeAs_2$. *Chem. Mater.* **2017**, *29*, 9300−9307.
(57) Chang, C.; Wu, M.; He, D.; Pei, Y.; Wu, C.-F.; Wu, X.; Yu, H.; Zhu, F.; Wang, K.; Chen, Y.; Huang, L.; Li, J.-F.; He, J.; Zhao, L.-D. 3D Charge and 2D Phonon Transports Leading to High Out-of-Plane ZT in n-Type SnSe Crystals. *Science* **2018**, *360*, 778−783.
(58) Madsen, G. K. Automated search for new thermoelectric materials: the case of LiZnSb. *J. Am. Chem. Soc.* **2006**, *128*, 12140−12146.
(59) Bilc, D. I.; Hautier, G.; Waroquiers, D.; Rignanese, G.-M.; Ghosez, P. Low-Dimensional Transport and Large Thermoelectric Power Factors in Bulk Semiconductors by Band Engineering of Highly Directional Electronic States. *Phys. Rev. Lett.* **2015**, *114*, 136601.
(60) He, J.; Amsler, M.; Xia, Y.; Naghavi, S. S.; Hegde, V. I.; Hao, S.; Goedecker, S.; Ozoliņš, V.; Wolverton, C. Ultralow Thermal Conductivity in Full Heusler Semiconductors. *Phys. Rev. Lett.* **2016**, *117*, 046602.
(61) Hu, X.; Jood, P.; Ohta, M.; Kunii, M.; Nagase, K.; Nishiate, H.; Kanatzidis, M. G.; Yamamoto, A. Power generation from nanostructured PbTe-based thermoelectrics: comprehensive development from materials to modules. *Energy Environ. Sci.* **2016**, *9*, 517−529.
(62) Zhao, L.-D.; Lo, S.-H.; Zhang, Y.; Sun, H.; Tan, G.; Uher, C.; Wolverton, C.; Dravid, V. P.; Kanatzidis, M. G. Ultralow thermal conductivity and high thermoelectric figure of merit in SnSe crystals. *Nature* **2014**, *508*, 373−377.
(63) Kuroki, K.; Arita, R. Pudding Mold" Band Drives Large Thermopower in $NaxCoO_2$. *J. Phys. Soc. Jpn.* **2007**, *76*, 083707.
(64) Xi, J.; Long, M.; Tang, L.; Wang, D.; Shuai, Z. First-principles prediction of charge mobility in carbon and organic nanomaterials. *Nanoscale* **2012**, *4*, 4348−4369.
(65) Long, M.-Q.; Tang, L.; Wang, D.; Wang, L.; Shuai, Z. Theoretical predictions of size-dependent carrier mobility and polarity in graphene. *J. Am. Chem. Soc.* **2009**, *131*, 17728−17729.
(66) Cai, Y.; Zhang, G.; Zhang, Y.-W. Polarity-reversed robust carrier mobility in monolayer MoS_2 nanoribbons. *J. Am. Chem. Soc.* **2014**, *136*, 6269−6275.
(67) Yang, J.-H.; Zhang, Y.; Yin, W.-J.; Gong, X.; Yakobson, B. I.; Wei, S.-H. Two-dimensional SiS layers with promising electronic and optoelectronic properties: theoretical prediction. *Nano Lett.* **2016**, *16*, 1110−1117.
(68) Zhu, Z.; Cai, X.; Yi, S.; Chen, J.; Dai, Y.; Niu, C.; Guo, Z.; Xie, M.; Liu, F.; Cho, J.-H.; Jia, Y.; Zhang, Z. Multivalency-Driven Formation of Te-Based Monolayer Materials: A Combined First-Principles and Experimental study. *Phys. Rev. Lett.* **2017**, *119*, 106101.
(69) Popescu, A.; Woods, L. M.; Martin, J.; Nolas, G. S. Model of transport properties of thermoelectric nanocomposite materials. *Phys. Rev. B: Condens. Matter Mater. Phys.* **2009**, *79*, 205302.
(70) Bahk, J.-H.; Bian, Z.; Shakouri, A. Electron energy filtering by a nonplanar potential to enhance the thermoelectric power factor in bulk materials. *Phys. Rev. B: Condens. Matter Mater. Phys.* **2013**, *87*, 075204.
(71) Hao, S.; Shi, F.; Dravid, V. P.; Kanatzidis, M. G.; Wolverton, C. Computational prediction of high thermoelectric performance in hole doped layered GeSe. *Chem. Mater.* **2016**, *28*, 3218−3226.
(72) Poncé, S.; Margine, E. R.; Verdi, C.; Giustino, F. EPW: Electron-phonon coupling, transport and superconducting properties using maximally localized Wannier functions. *Comput. Phys. Commun.* **2016**, *209*, 116−133.
(73) Zhou, J.-J.; Park, J.; Lu, I.-T.; Maliyov, I.; Tong, X.; Bernardi, M. Perturbo: a software package for ab initio electron-phonon interactions, charge transport and ultrafast dynamics. *arXiv Preprint (Condensed Matter: Materials Science)*: 2020. arXiv:2002.02045. https://perturbo-code.github.io/

https://doi.org/10.1021/acsaelm.0c01100
ACS Appl. Electron. Mater. 2021, 3, 1610−1620